Available online at www.sciencedirect.com
SCIENCE DIRECT®
Thermochimica Acta 426 (2005) 207–212
thermochimica acta
www.elsevier.com/locate/tca

# Phase transitions in octanethiol-capped Ag nanocluster microfilm assemblies

A.V. Ellis[a,b], J. D'Arcy-Gall[a], K. Vijayamohanan[a,c], R. Goswami[a], P.G. Ganesan[a], C. Ryu[d], G. Ramanath[a,*]

[a] *Materials Science and Engineering Department, Rensselaer Polytechnic Institute, Troy, NY 12180, USA*
[b] *Department of Physics, New Mexico State University, P.O. Box 30001, Las Cruces, NM 88001, USA*
[c] *National Chemical Laboratory, Pune, India*
[d] *Chemistry Department, Rensselaer Polytechnic Institute, Troy, NY 12180, USA*

Received 27 April 2004; received in revised form 30 July 2004; accepted 2 August 2004
Available online 11 September 2004

**Abstract**

We describe phase transitions in microfilm assemblies of octanethiol (OT)-capped 2–4 nm-diameter Ag nanoclusters prepared from solutions with OT/$Ag^+$ ratios of ∼50. Using DSC we observe two melting/crystallization-type reversible phase transitions: one at ∼61 °C due to interdigiated unattached octanethiol, and the other at ∼125 °C due to the phase comprised of the assembly of OT-capped nanoclusters. Increased thermal fluctuations weaken the inter-chain hydrophobic interactions between interdigitated OT molecules, leading to both phase transitions. The thiolate bond of OT-molecules bound to Ag nanoclusters are more rigid, thereby requiring a higher temperature to increase the flexibility of the alkyl chain of OT, and to melt the nanocluster assembly. The mobility of the nanoclusters in the melt is limited, and morphological features of the original assemblies are retained during recrystallization. No observable mass loss is detected up to ∼180 °C, above which OT molecules desorb from the Ag nanoclusters.


*Keywords:* Silver nanoclusters; Differential thermal analysis; Infrared spectroscopy; Phase transitions

## 1. Introduction

Metal/semiconductor nanoclusters are considered to be attractive building blocks for constructing nanoelectronic devices due to their unique size-dependent, and often tunable, thermal, optical, electronic and magnetic properties arising from quantum confinement effects. In particular, there has been a great deal of interest in creating ordered assemblies of nanoclusters of select sizes, arranged in specific configurations for reaping the benefits of these properties in potential applications such as sensors, catalysis, nonlinear optics and single electron devices [1–6]. For example, assembling arrays of alternating small and large sized semiconductor nanoclusters can give rise to resonant tunneling effects that could be harnessed in nanodevices for optical applications [1]. It is critical to understand the thermal and chemical stability of such nanocluster assemblies because their size- and organization-dependent functional properties are sensitive to phenomena such as coalescence and disordering.

Nanoclusters that are isolated from each other, e.g., by capping agents, tend to coalesce slower than their uncapped counterparts, and hence, are structurally and electronically more stable. Typically these types of "protected" or "passivated" nanoclusters can be prepared by a variety of methods, including hydrolysis and reduction of precursors [7,8], thermal decomposition [9], photolysis [10] and nanosphere lithography [11]. One common method of protecting the clusters is to attach amphiphilic molecules such as alkyl thiols to the nanocluster surfaces. This technique is versatile, and has

* Corresponding author. Tel.: +1 518 276 6844; fax: +1 518 276 8554.
*E-mail address:* ramanath@rpi.edu (G. Ramanath).

0040-6031/$ – see front matter © 2004 Elsevier B.V. All rights reserved.
doi:10.1016/j.tca.2004.08.009

been used to synthesize clusters of single metals [12–14], alloys [15,16] and semiconductors [4,17]. In this technique, it is essential to obtain maximal and uniform coverage of the self-assembled molecular layers on the nanocluster surfaces to effectively protect the nanoclusters. Conformal packing also produces strong binding asymmetry and facilitates lateral van der Waals-type interactions between chains of adjacent molecules, thereby further inhibiting species penetration through the capping layer and oxidative processes on the nanocluster surfaces [18,19]. Thin films of these conformal packed structures have application in chemical sensing in devices such as metal-insulator–metal-ensembles (MIMEs) in which tailored selectivities can be established by adjusting nanocluster type and passivant ligand.

In this work we investigate the thermal stability of microfilm assemblies of octanethiol (OT)-capped Ag nanoclusters obtained from solutions with high OT/$Ag^+$ ratios using a combination of calorimetry, optical and electron spectroscopy and microscopy techniques. By producing microfilms of these assemblies we observed that two phases exsisted. One phase is an ordered assembly of Ag nanoclusters held together by interdigitation of OT molecules chemisorbed onto the nanocluster surfaces through a thiolate bond. The other phase consists of excess OT molecules that are not directly attached to Ag nanoclusters, but are linked to each other, and the chemisorbed OT-caps on the Ag nanoclusters, through van der Waals interteractions and are an intergal part in the film formation. Both phases have a melting/crystallization phase transition with no mass loss over the temperature range studied.

## 2. Experimental

Using an adaptation of the Brust method [20] we prepared microfilms of Ag nanoclusters capped with octanethiol (OT), by reducing metal salts from a two-phase liquid mixture. In order to produce smaller particle sizes and maximize thiolate bond coverage on nanoclusters we use solutions with high (e.g., ∼50) OT/$Ag^+$ ratios. We note that the OT itself acts as a phase transfer agent, obviating the need for additional agents such as tetra *n*-octylammonium bromide [14,15].

The capped nanoclusters were prepared from a mixture of equal volumes of 1 mM aqueous $AgNO_3$ and 46 mM octanethiol in toluene. The biphasic mixture was placed in an ice-bath at 5 °C, and stirred vigorously with a magnet rotating at 600 rpm. A 7.4 mM aqueous solution of $NaBH_4$ was slowly added to the mixture, resulting in OT-capped nanoclusters that migrate to the toluene layer. The toluene layer containing the OT-capped nanoclusters was separated from the bottom aqueous layer using a separating funnel, washed five times with deionized water, and dried in flowing $N_2$. In order to obtain continuous films rather than separate nanoclusters we negated the use of precipitation induced by methanol addition. These thin films were then used for analysis.

The nanocluster size, intercluster spacings and structural packing of the assemblies were characterized by transmission electron microcopy (TEM) after being transferred onto a carbon-coated Cu-grid. A JEOL-2010 instrument operated at 200 kV was used for these measurements. Differential scanning calorimetry (DSC) measurements were carried out in a Mettler Toledo model DSC822$^e$ instrument (calibrated with indium) to investigate phase changes in the nanocluster assemblies during heating and cooling. Thermograms were collected on ∼3 mg samples sealed in aluminum pans under 40 mL/min $N_2$. Each sample was repeatedly heated from 0 to 150 °C at 10 °C/min, and cooled to −30 °C at different rates between −5 and −30 °C/min. Calorimetric data was extracted by fitting the area under the endotherm and exotherm peaks.

We carried out thermogravimetric analysis (TGA) on 5–10 mg samples in a Mettler Toledo TGA/SDTA851$^e$ instrument to track desorption and decomposition processes. Each sample was heated from 25 to 800 °C at 10 °C/min under 20 mL/min $N_2$.

In situ polarized light microscopy (PLM) was used to visually capture and correlate phase changes in the nanocluster assemblies with measured DSC peaks. The PLM measurements were carried out on the nanocluster assemblies heated at 1 °C/min to 150 °C in a Nikon Eclipse E 600 Microscope equipped with a Linkam TMS (93) heating stage.

Microscope reflectance infrared (IR) spectroscopy enabled monitoring of changes in the octanethiol assembly both before and after thermal treatment. A Spectratech IR-Plan Advantage microscope computer-interfaced with a Nicolet Magna Fourier transform IR 560 spectrophotometer was used for our measurements. The results reported here were obtained from 200 scans at a 2 $cm^{-1}$ resolution. Background spectra were collected on a glass slide coated with 100 μm of gold and subtracted from the sample spectra.

## 3. Results

### 3.1. High resolution transmission electron microscopy (HRTEM)

Fig. 1a shows a typical bright-field TEM micrograph of a OT-capped Ag nanocluster film assembly. The Ag nanoclusters have an fcc crystal structure with a lattice parameter of 0.408 nm, identical to that of bulk Ag, as indicated by the representative diffraction pattern and the high resolution TEM micrograph shown in Fig. 1b and c, respectively. The concentric of the {1 1 1} planes seen in the HRTEM micrograph are identical to that of bulk Ag. Analysis of approximately 40 clusters the TEM micrographs shows that the nanocluster sizes range from ∼2.7 to 6.2 nm, with the highest frequency at ∼4 nm (see Fig. 1d).

The intercluster spacings, estimated by constructing Voronoi [21,22] cells around each cluster in close-packed assemblies, yield discrete values with high frequencies be-

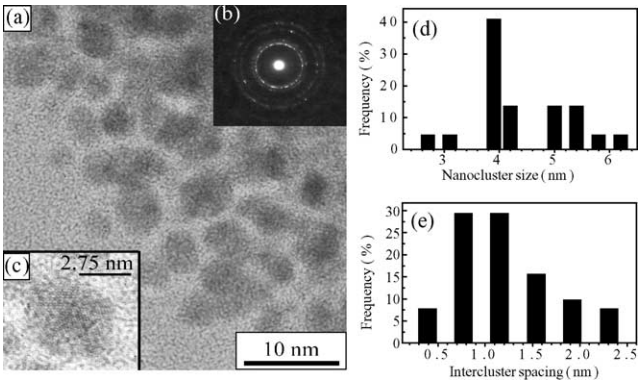


Fig. 1. (a) TEM micrograph of as-prepared OT-capped Ag nanoclusters; (b) diffraction pattern showing (1 1 1), (2 0 0), (2 2 0) and (3 1 1) reflections from fcc Ag; (c) HRTEM image of a Ag nanocluster showing {1 1 1} lattice fringes. Histograms of (d) the Ag nanocluster size distribution and (e) spacings between nearest-neighbor nanoclusters.

tween ∼0.7 and 1.2 nm (see Fig. 1e). This intercluster spacing range correlates well with one- to two-times the length of OT molecules (0.7 nm), indicating interdigitation of 2–4 overlapping methyl groups in OT molecules capping adjacent nanoclusters. This is expected to result in hydrophobic interactions between the OT caps, as described previously [23]. Spacings higher than ∼2 nm most likely arise from clusters separated by regions of excess interdigitated OT-molecules that are not directly attached to the nanocluster surfaces. We attribute the small size of our clusters to the high thiol/metal-ion ratio in which after initial nucleation passivation occurs rapidly thereby inhibiting further particle growth.

### 3.2. IR spectroscopy

The conformation and environment of the OT capping agents in the Ag nanocluster microfilm assembly was characterized by IR spectroscopy. Fig. 2 shows the low-frequency (600–1600 $cm^{-1}$) and the high-frequency (2800–3000 $cm^{-1}$) regions of the spectra. The asymmetric and symmetric $-CH_3$ stretching modes at 2920 and 2842 $cm^{-1}$, respectively, indicate that the alkyl chains are mostly all-*trans* extended in a close-packed configuration with a high degree of molecular interdigitation. This inference is confirmed by the absence of strong end-gauche defect signatures at ∼1341 $cm^{-1}$. This molecular configuration maximizes van der Waals forces and gives rise to a high degree of rotational and vibrational confinement [23] of the amphiphillic OT molecules. While $-CH_3$ modes at 2957 and 2974 $cm^{-1}$ arise from the relative orientational freedom of the chain termini, the absence of splitting in the asymmetric $-CH_3$ mode suggests hindered chain rotations about OT chain axis. Equidistant bands in the 1150–1350 $cm^{-1}$ region of the spectra, due to out-of-plane C–H twisting and wagging vibrations, suggest the presence of a crystalline OT phase. Splitting of the $CH_2r$ ($CH_2$ in-plane rocking mode) into two distinct unequal bands at 721 and 732 $cm^{-1}$, observed in our spectra, also supports the presence of crystalline OT. Similar observations have been attributed to

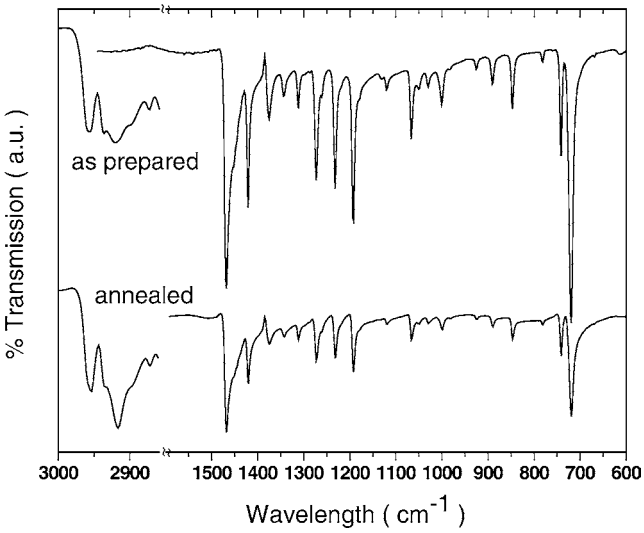


Fig. 2. IR spectra of OT capped-Ag nanoclusters in the as-prepared form, and after annealing to 150 °C.

the presence of alkyl chains with orthorhombic packing [22]. These results indicate the presence of an additional phase comprised of excess OT molecules. This inference is supported by the DSC and TGA measurements. Spectra from assemblies annealed to 150 °C and cooled to room temperature (also shown in Fig. 2) were essentially identical to that obtained from as-prepared assemblies. The presence of odd numbered alkyl chains before and after annealing indicated by $CH_3$–C methyl rocking bands (normally inactive in even-numbered alkanes) at 1375 and 1120 $cm^{-1}$ indicate that the structure of the OT chains do not undergo degradation due to condensation or branching side reactions during annealing at these temperatures.

### 3.3. DSC and TGA

The nanocluster microfilm assembly was heated from 0 to 150 °C to investigate its thermal stability. The heating rate was 10 °C/min for all scans, while the cooling rates were varied between −5 and −30 °C/min. During heating, the DSC spectra shown in Fig. 3a and b exhibit two endothermic

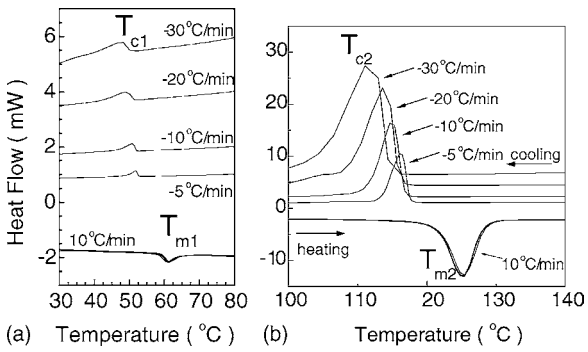


Fig. 3. DSC thermograms of multiple runs of thermally cycled OT capped-Ag nanoclusters shown between (a) 30 and 80 °C and (b) 100 and 150 °C.

Table 1
Transition temperatures and enthalpies extracted from DSC results

| Endotherm $T_{m1}$ (°C) | $\Delta H_{m1}$ (J/g) | Exotherm $T_{c1}$ (°C) | $\Delta H_{c1}$ (J/g) | Endotherm $T_{m2}$ (°C) | $\Delta H_{m2}$ (J/g) | Exotherm $T_{c2}$ (°C) | $\Delta H_{c2}$ (J/g) |
|---|---|---|---|---|---|---|---|
| 61.26 | 18.96 | 51.70 | 18.24 | 125.46 | 101.82 | 116.09 | 102.78 |
| 61.26 | 18.17 | 50.73 | 18.28 | 125.46 | 103.23 | 114.65 | 102.81 |
| 61.26 | 18.19 | 48.78 | 17.89 | 125.46 | 101.41 | 113.58 | 102.23 |
| 60.59 | 18.18 | 48.17 | 17.38 | 124.79 | 102.59 | 111.07 | 101.96 |

peaks $T_{m1}$ and $T_{m2}$ located at ∼61 and ∼125 °C, respectively. During cooling at −10 °C/min, we observe two exothermic peaks, $T_{c1}$ and $T_{c2}$ at ∼50 and 115 °C, respectively. Both the exotherms and the endotherms were observed during repeated heating and cooling, as shown in (see Fig. 3a and b) indicating that both transitions are reversible. While increasing the cooling rate results in a small decrease in the endothermic transition temperatures, there are no observable changes in the enthalpy values (see Table 1) extracted from the area of the peaks corresponding to the respective transitions. The low-temperature ($T_{m1}$) endothermic peak at ∼61 °C corresponds to the "melting" of the phase consisting of excess interdigitated alkanethiols that are not directly attached to the nanocluster surfaces, but are intercalated between the clusters in a crystalline form. Typically OT is a liquid at room temperature, however this intercalation to form a solid crystalline form has dramatically changed its melting point [13]. This solid form holds the nanoclusters in the microfilm array at temperatures up to its first melting transition of ∼61 °C. The crystallization exotherms at $T_{c1}$ are similar to that reported for a crystalline phase consisting of octadecanethiol (∼66 °C) reported previously [13].

The presence of this solid phase comprised of interdigitated OT molecules, between OT-capped nanoclusters, is corroborated by our IR spectroscopy results indicating the presence of crystalline OT. The high-temperature ($T_{m2}$) endothermic peak located at 125 °C is due to the increased flexibility of the interdigitated chains of OT that are chemisorbed onto the nanocluster surfaces. The enthalpy values observed here are in agreement with previously reported values for OT-capped Ag nanoclusters [12,13]. The lack of any observable changes in the enthalpy data after each cycle suggests that there are no significant changes in the ordering or defect densities in these assemblies. We note that the Ag clusters themselves are intact and do not melt at these temperatures. Heating above 180 °C leads to the disappearance of the phase transition exotherms and the endotherms during subsequent DSC cooling and heating. We carried out TGA measurements from 0 to 800 °C.

Fig. 4 shows that there is a 55 wt.% mass loss of the original material between 180 and 300 °C. There is no observable mass loss below 180 °C, or between 300 and 800 °C. These results indicate that about 55 wt.% of the Ag–OT nanocluster assembly is comprised of OT, consistent with the high OT/$Ag^+$ ratios used in our experiments. Prior works suggest [24] that only ∼20–25 wt.% mass loss can account for directly capping nanoclusters of sizes similar to ours, corroborating the presence of a phase comprised of excess OT

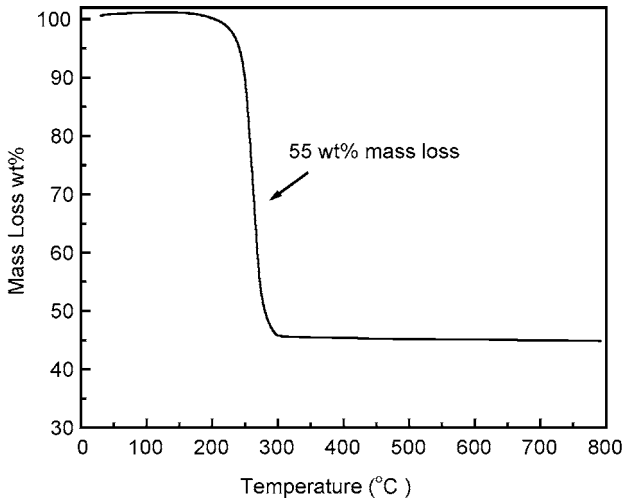


Fig. 4. TGA profile of OT capped-Ag nanoclusters heated from 0 to 800 °C.

holding the assembly in a solid microfilm. At ∼180 °C, the OT desorbs from nanocluster surfaces and paves the way for irreversible aggregation of the silver clusters through coalescence, as reported earlier [25]. These desorbed molecules decompose between 180 and 300 °C.

### 3.4. In situ polarized light microscopy (PLM)

In situ PLM measurements showed the morphological changes occurring during the above phase transitions. In this technique, changes in the contrast features reveal crystalline–amorphous transitions. PLM micrographs obtained from Ag nanocluster assemblies during heating, and cooling, are shown in Figs. 5a–e and 6f–j, respectively. At temperatures below ∼61 °C PLM micrographs consist of brown- and white-colored regions corresponding to birefringent crystalline phases, amidst dark contrast regions of optically isotropic material (Fig. 5a). It is most likely that the optically isotropic regions are amorphous or disordered assemblies of excess OT molecules that are not directly attached to the Ag nanoclusters.

Upon heating to ∼61 °C, the dark brown-colored regions begin to become discontinuous and expose regions (size range: ∼few μm to several tens of μm) of white contrast beneath them (see arrows in 5b). In the light of the DSC, IR and TGA results, this observation indicates that the brown regions correspond to crystalline domains of excess thiol, and the white regions correspond to the nanocluster assemblies. This is verified by the samples showing mainly white and

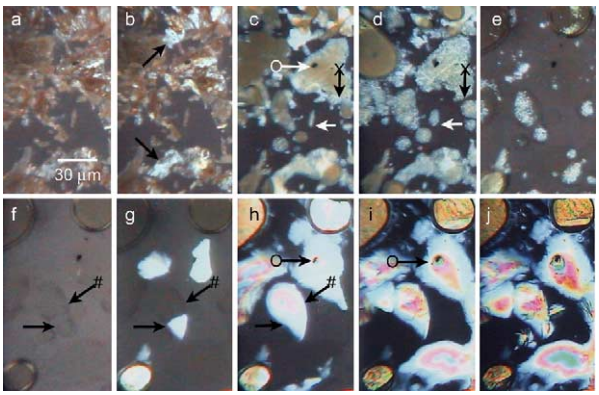


Fig. 5. In situ PLM micrographs obtained from OT capped-Ag nanoclusters at (a) 43 °C, (b) 61 °C, (c) 120 °C, (d) 125 °C, (e) 127 °C and (f) 130 °C during heating; and (g) 121 °C and (h) 119 °C, (i) 117 °C and (j) 107 °C during cooling.

dark contrast domains between 61 and 120 °C. Fig. 5c shows an example micrograph taken at 120 °C. Traces of brown regions seen on the nanocluster assemblies (white) are due to remnant excess OT molecules interdigitated with those chemisorbed onto the nanoclusters.

At ∼125 °C, the nanocluster assemblies (white) begin to breakup through formation of disordered regions (dark). For example, the black strait—indicated by the X-tailed arrow in Fig. 5d—between two nanocluster assembly islands is absent at the same location at 120 °C (see X-tailed arrow in Fig. 5c). A comparison of Fig. 5c and d reveal two other features: the disappearance of brown contrast traces on the nanoclusters at ∼125 °C, and increased mobility of nanoclusters. The latter is reflected by shape changes of the nanocluster assembly islands (e.g., see left-pointing horizontal arrows in Fig. 5c and d). Both these effects are due to weakened hydrophobic interactions between interdigitated OT molecules and increased molecular flexibility. Further heating results in the destruction of the crystalline order (i.e., melting) of the assemblies, as indicated by the abrupt decrease, and disappearance of phase contrast (see Fig. 5e and f). We can, however, discern faint contours of the islands of nanocluster assemblies (e.g., those indicated by horizontal arrow and the #-tailed arrow in Fig. 5f). Upon cooling below 122 °C the nanocluster assemblies recrystallize as shown in Fig. 5g and h. While the shapes of the crystallites are, in general, different from those observed in the original sample, in many cases they exhibit memory of the previous islands' features.

For example, the crystallites indicated by the horizontal arrow and the #-tailed arrow in Fig. 5g and h broadly conform to the outline of the previous island (in Fig. 5f). We also note the retention of the size, location and shape of entrapped regions of excess thiols during recrystallization; compare dark-contrast spot indicated by O-tailed arrows in Fig. 5h and i on the one hand, and 5c on the other. These observations suggest that even though the nanocluster assembly has melted, the mobility of the nanoclusters is confined to no more than a few μm. Traces of the dark brown/red regions reappear at

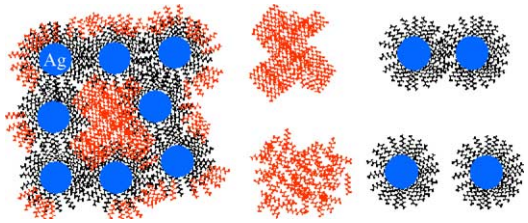


Fig. 6. Schematic illustration of the microstructure and phase transitions in OT–Ag nanocluster assemblies prepared from high thiol/metal-ion ratio solutions. Left: nanocluster (blue) assembly held together via interdigitation of chemisorbed OT (black). Also shown are assemblies of excess OT (red) not directly attached to the nanoclusters. Center: disordering of the crystalline portions of the excess OT phase. Right: nanocluster assembly melting due to disengagement of interdigiated OT chemisorbed onto adjacent clusters. Both the transitions are reversible upon cooling.

∼117 °C (see Fig. 5i and j), and proliferate upon cooling below 61 °C. leading to a view similar to that seen in Fig. 5a. The excellent correlation between the temperatures at which the major contrast changes are observed, and the transition temperatures measured by DSC further confirm the labeling of the colors with the respective crystalline phases. The reversibility of PLM contrast and phase transitions indicated by DSC, and the lack of mass loss below 150 °C indicate that both transitions are caused by changes in mobility of the OT molecules. The higher temperature of the melting of the nanocluster assembly is most likely due to the enhanced rigidity of the OT molecules due to the strong Ag–S bond between the nanoclusters and OT.

## 4. Discussion and conclusions

Based upon the above results we propose a phenomenological description of the Ag nanocluster microfilm assembly and its thermal behavior. The key elements of this model are schematically illustrated in Fig. 6. The high thiol to metal ion ratio leads to the formation of two solid phases in the microfilm. One phase consists of assemblies of fcc Ag nanoclusters (blue spheres) capped with chemisorbed OT (black) on their surfaces. The nanoclusters are interlinked to each other through hydrophobic interactions via interdigitation of chemisorbed OT-molecules on adjacent nanoclusters. Ordered domains of a second phase (red) interspersed between the nanocluster assembly are comprised of excess thiols that are not directly linked to the nanoclusters. Both phases are held together by hydrophobic interactions via molecular interdigitation between adjacent OT molecules to form an extented solid-state film. Annealing to ∼61 °C melts the crystalline portions of the excess OT phase due to increased molecular flexibility and decreased hydrophobic interactions (see Fig. 6 center). The flexibility of the chemisorbed OT increases at a higher temperature of ∼125 °C because the strong Ag–S bond on the nanocluster surface makes the molecule relatively rigid.

This leads to decoupling of the interdigitated OT molecules of adjacent clusters leading to the melting of the Ag

nanocluster assembly (see Fig. 6 right). Both these transitions are reversible, and do not involve structural changes in the Ag clusters or the OT. The mobility of the nanoclusters in the melt is limited, suggested by the retention of morphological features of the original assembly. Upon heating above 150 °C, both phase transitions disappear upon subsequent cooling and reheating due to OT desorption and intramolecular cleavage, and cluster coalescence.

## Acknowledgements

We gratefully acknowledge funding from Philip Morris USA, NY state and NSF-CAREER Award DMR 994478.

## References

[1] O. Kulakovich, N. Strekal, A. Yaroshevich, S. Maskevich, S. Gaponenko, I. Nabiev, U. Woggon, M. Artemyev, Nano Lett. 2 (2002) 1449.
[2] S.P. Gubin, Y.V. Gulayev, G.B. Khomutov, V.V. Kislov, V.V. Kolesov, E.S. Soldatov, K.S. Sulaimankulova, A.S. Trifonov, Nanotechnology 13 (2002) 185.
[3] J.P. Wilcoxon, P. Newcomer, in: Proceedings of SPIE—The International Society for Optical Engineering, vol. 4808, 2002, p. 99.
[4] J. Aldana, A. Wang, X. Peng, J. Am. Chem. Soc. 123 (2001) 8844.
[5] S.-H. Kim, G. Medeiros-Ribeiro, D.A.A. Ohlberg, R. Stanley Williams, J.R. Heath, J. Phys. Chem. B 103 (1999) 10341.
[6] D.J. Schriffrin, MRS Bull. (2001) 1015 (Dec.).
[7] S. Pethkar, M. Aslam, I.S. Mulla, P. Ganeshan, K. Vijayamohanan, Mater. Chem. 11 (2001) 1710.
[8] A.V. Ellis, K. Vijayamohanan, C. Ryu, G. Ramanath, Mater. Res. Soc. Symp. Proc. 739 (2003), H6.4.1.
[9] H. Nagasawa, M. Maruyama, T. Komatsu, S. Isoda, T. Kobayashi, Phys. Status Solidi A: Appl. Res. 191 (2002) 67.
[10] L.A. Peyser, T.-H. Lee, R.M. Dickson, J. Phys. Chem. B 106 (2002) 7725.
[11] T.R. Jensen, G.C. Schatz, R.P.J. van Duyne, Phys. Chem. B 103 (1999) 2394.
[12] N. Sandhyarani, M.R. Resmi, R. Unnikrishnan, K. Vidyasagar, S. Ma, M.P. Antony, G.P. Selvam, V. Visalakshi, N. Chandrakumar, K. Pandian, Y.-T. Ta, T. Pradeep, Chem. Mater. 12 (2000) 104.
[13] N. Sandhyarani, M.P. Antony, G.P. Selvam, T.J. Pradeep, Chem. Phys. 113 (2000) 9794.
[14] N.K. Chaki, S.G. Sudrik, H.R. Sonawane, K. Vijayamohanan, Chem. Commun. 1 (2002) 76.
[15] N. Sandhyarani, T. Pradeep, Chem. Mater. 12 (2000) 1755.
[16] R. Philip, S. Mujumdar, H. Ramachandran, G.R. Kumar, N. Sandhyarani, T. Pradeep, MCLC S & T Sec. B: Nonlinear Opt. 27 (2001) 357.
[17] R.B. Khomane, A. Manna, A.B. Mandale, B.D. Kulkarni, Langmuir 18 (2002) 8237.
[18] P.E. Laininis, G.M. Whitesides, J. Am. Chem. Soc. 114 (1992) 9022.
[19] Z. Mekhalif, J. Riga, J.-J. Pireaux, J. Delhalle, Langmuir 13 (1997) 2285.
[20] M. Brust, M. Walker, D. Bethell, D.J. Schriffrin, R. Whyman, J. Chem. Soc., Chem. Commun. (1994) 801.
[21] A.V. Ellis, K. Vijayamohanan, R. Goswami, N. Chakrapani, L.S. Ramanathan, P.M. Ajayan, G. Ramanath, Nano Lett. 3 (2003) 279.
[22] M. Nygards, P. Gudmundson, Mater. Sci. Eng. A 325 (2002) 435.
[23] R.W. Meulenberg, G.F. Strouse, J. Phys. Chem. 105 (2001) 7438.
[24] R.H. Terrill, T.A. Postlethwaite, C.-H. Chen, C.-D. Poon, A. Terzis, A. Chen, J.E. Hutchison, M.R. Clark, G. Wignall, J.D. Londono, R. Superfine, M. Falvo, C.S. Johnson Jr., E.T. Samulski, R.W. Mury, J. Am. Chem. Soc. 117 (1995) 12537.
[25] B.A. Korgel, N. Zaccheroni, D.J. Fitzmaurice, J. Am. Chem. Soc. 121 (1999) 3533.